Available online at www.sciencedirect.com
SCIENCE DIRECT®
Journal of Solid State Chemistry 175 (2003) 159–169
JOURNAL OF SOLID STATE CHEMISTRY
http://elsevier.com/locate/jssc

Textural and structural properties and surface acidity characterization of mesoporous silica-zirconia molecular sieves

E. Rodríguez-Castellón,[a] A. Jiménez-López,[a,*] P. Maireles-Torres,[a] D.J. Jones,[b] J. Rozière,[b] M. Trombetta,[c] G. Busca,[c] M. Lenarda,[d] and L. Storaro[d]

[a] *Departamento de Química Inorgánica, Cristalografía y Mineralogía, Universidad de Málaga, Apdo. 59, 29071 Málaga, Spain*
[b] *Laboratoire des Agrégats Moléculaires et Matériaux Inorganiques, UMR CNRS 5072 Université Montpellier II, 34095, Montpellier, France*
[c] *Dipartimento di Ingegneria Chimica e di Processo, Università di Genova, Ple. J.F. Kennedy, I-16129 Genova, Italy*
[d] *Dipartimento di Chimica, Università di Venezia Ca'Foscari, Dorsoduro 2137-30123 Venezia, Italy*

Received 11 November 2002; received in revised form 28 January 2003; accepted 14 April 2003

Abstract

Homogeneous mesoporous zirconium-containing MCM-41 type silica were prepared by supramolecular templating and their textural and structural properties were studied using powder X-ray diffraction, N_2 porosimetry, atomic force microscopy, EXAFS, XPS, and UV–VIS–NIR diffuse reflectance spectroscopy. Their acid properties were also studied by using IR spectroscopy and by the use of catalytic tests such as the decomposition of isopropanol and the isomerization of 1-butene. The materials prepared show a good degree of crystallinity with a regular ordering of the pores into a hexagonal arrangement and high thermal stability. The specific surface area of the prepared materials decreases as the zirconium content rises. Zirconium atoms are in coordination 7 to 8 and located at the surface of the pores such that a high proportion of the oxygen atoms bonded to zirconium corresponds to surface non-condensed oxygen atoms. Both facts are responsible for the acid properties of the solids that show weak Brønsted and medium strong Lewis acidity.
© 2003 Elsevier Inc. All rights reserved.

Keywords: MCM-41; Zirconium; Mesoporous silica AFM; EXAFS; Acid properties

1. Introduction

In structurally microporous solids such as aluminosilicate zeolites [1] and aluminophosphate based materials [2,3], sites with a particular reactivity (such as cations for metal exchanged zeolites and highly acidic protons for hydrogen-form zeolites) give rise to very efficient adsorption and catalytic activities [4,5]. The application of such porous materials to certain heterogeneous catalytic reactions can be limited, for example, by high reactivity of their sites (as for a solid Brønsted acid giving rise to cracking and coking) or an insufficiently large cavity size.

Aluminum-containing MCM-41 mesoporous silicas [6–8] were found particularly useful as acid catalysts in reactions [9–11]) such as *n*-alkane, olefin and methyl-aromatics skeletal isomerizations, oligomerization, alkylation, cracking and hydrocracking [12,13]. Metal-containing mesoporous solids have been recently used as catalysts for organic reactions [14] and, for example, an unusual selective oxidation of linear alkanes by molecular oxygen has been reported [15].

As is now well-known [6,7], the formation of the hexagonal arrangement of mesoporous channels in MCM-41 is controlled by the structure directing action of appropriate concentrations of cationic surfactants. These molecules can, in principle, generate a mesoporosity in several different synthetic amorphous materials.

Zirconia has recently been proposed as a promising component of catalysts for hydrotreatment [16], for the selective catalytic reduction of NO_x by ammonia [17] and, when sulfated [18], or combined with tungsten oxide [19], for acid catalysis. The association of a regular mesoporous structure and the particular surface acid characteristics contributed by the presence of zirconium is of particular interest. A preliminary communication on the preparation in basic and acidic media of zirconium doped mesoporous silica containing Si/Zr ratios in the range 50–5, as well as surface characterization of the

*Corresponding author. Fax: +34952132000.
E-mail address: ajimenezl@uma.es (E. Rodríguez-Castellón).

0022-4596/03/$ - see front matter © 2003 Elsevier Inc. All rights reserved.
doi:10.1016/S0022-4596(03)00218-4

materials synthesized was published by some of us [20]. We have also recently reported catalytic applications either catalysts in the vapor phase synthesis of alkylindoles [21] or supports of chromia for the oxidative dehydrogenation of propane [22], metallic nickel for the gas-phase hydrogenation of nitriles [23] and cobalt oxide for the selective catalytic reduction of NO with ammonia [24]. Other authors have prepared similar materials using either molecular or ionic precursors [25–28], and activity in redox catalysis has been reported [28–29]. Recent articles have extended the study of the preparation of mesoporous silica-zirconia at low pH and using ionic (rather than molecular) precursors [30] and hydrothermal conditions at 383 K [31]. We describe now a more complete study of bulk structural and surface textural and specially the acidic properties as a function of the zirconium content of mesoporous silica-zirconia, and compare surface acidity characteristics with those of MCM-41 silica and an aluminosilicate prepared using a similar micelle templating route.

2. Experimental section

2.1. Sample preparation

2.1.1. Si/Zr samples

Chemicals were supplied by Aldrich and were used as received. Zirconium-containing mesoporous MCM-41-type silica was prepared by adding appropriate amounts of tetraethoxysilane and zirconium *n*-propoxide to an ethanol–propanol solution, which was stirred at room temperature for 15 min, and then added to an aqueous solution of hexadecyltrimethylammonium bromide (25 wt%), previously stirred at 353 K for 30 min. The surfactant/($SiO_2 + ZrO_2$) ratio was 0.5. The pH was adjusted to 10 by addition of an aqueous solution of tetramethylammonium hydroxide (25 wt%), and the resulting gels were stirred at room temperature for 4 days. Solid products were recovered by centrifugation, washed with ethanol, dried at 343 K, and then calcined in air at 823 K for 6 h (1 K min^{-1} heating rate) in order to remove the surfactant. Si/Zr molar ratios (R) of 40–5 were used, giving samples denoted SiZrR-T, where T is the temperature of the reaction medium: SiZr25–298 and SiZr5–298. In a similar way, SiZr5-353, SiZr5-373, SiZr5-423, SiZr30-373 and SiZr40-373 were prepared by stirring the synthesis gels first for 1 day at 353, 373 and 423 K, respectively, and then for 2 days at room temperature.

2.1.2. Si and Si/Al samples

MCM-41 was prepared using hexadecyltrimethylammonium bromide, NaOH (Janssen) and SiO_2 (Ludox® AS30) in a molar ratio Si/surfactant = 6. Crystallization of the gels was carried out in a Teflon-lined stainless steel autoclave at 383 K. After cooling, the product was filtered, washed with deionized water and dried at 353 K overnight. It was then ground, calcined in air flow at 823 K (heating rate 10 K/min) for 5 h, exchanged with 2 M NH_4Cl aqueous solution and finally calcined again to obtain a product free from Na^+ ion. Al-MCM41 was obtained following the above procedure modified by adding $NaAlO_2$ (Carlo Erba) to the gel to reach the ratio Si/Al = 5.

2.2. Materials characterization

Chemical analyses of Si and Zr were performed by atomic absorption spectroscopy on a Perkin-Elmer 3100 spectrometer. Powder X-ray diffraction (XRD) patterns were recorded on a Siemens D501 diffractometer using Cu$K\alpha$ radiation and a graphite monochromator. Nitrogen adsorption–desorption isotherms at 77 K of calcined samples were obtained using an automatic Carlo Erba 1800. BET specific surface areas were evaluated using 0.162 nm^2 as the cross-sectional area of the adsorbed nitrogen molecule. Pore size distributions were calculated with the Cranston and Inkley method for cylindrical pores [32]. Selected samples were topographically characterized using atomic force microscopy. Images were obtained at room temperature with Nanoprobe™ (Digital Instruments) tapping tips obtained from etched silicon, having a high aspect ratio, thus avoiding or minimizing convolution of the tip shape by the solid surface. Images were analyzed by a computerized procedure. Transmission electron micrographs were obtained with a JEOL 1200 EX microscope operating at 100 kV.

X-ray absorption spectra were measured on the spectrometer EXAFS13, line D42, at LURE (Paris Sud University), using synchrotron radiation and a double crystal monochromator with Si [311] crystals in the energy range of the zirconium K-edge ($E_0 = 17998$ eV). Energy calibration was made using a 20 μm Zr-foil by assigning E_0 to the inflection point in the absorption edge. EXAFS spectra were recorded with 2.0 eV step from ca. 100 eV before the edge to 900 eV after it. Experiments were performed in transmission mode using two ionization chambers filled with argon for the measurement of the X-ray intensity before and after the sample, I_0 and I_T, respectively.

Samples of reference ZrO_2 and $ZrSiO_4$, and of SiZr25-298 in the surfactant-containing mesophase, and after calcination were mulled to a thick paste with paraffin oil, pressed between two parafilm windows and fixed in a stainless sample holder. This was placed in a cold finger cryostat (77 K) under dynamic vacuum (~2 mbar). The amount of sample was calculated to give an edge jump $\Delta\mu$ ca. 1.

Experimental data were analyzed using computer codes developed by Michalowicz [33] using the analysis procedures described elsewhere [34]. These included: (i) extraction of the EXAFS signal $\chi(k)$ from the absorption spectrum $\mu(E)$ (ii) calculation of the EXAFS Fourier transform (FT) radial distribution-like function $F(R)$ (iii) filtering of the successive coordination spheres in $F(R)$ and calculation of their inverse Fourier transform to obtain partial components of the EXAFS spectra; (iv) multivariate least squares fitting of the filtered EXAFS spectra using photoelectron phase and amplitude functions calculated using FEFF7 [35]. The number of nearest neighbors, N_i, the inter-atomic absorber–neighbor distance, R_i, and the Debye–Waller-type factor, σ_i, were obtained for each coordination shell of atoms. In all cases, the fitting residue was lower than 2%.

X-ray photoelectron spectra were obtained using a Physical Electronics PHI 5700 spectrometer with non-monochromatic Mg$K\alpha$ radiation (300 W, 15 kV, 1253.6 eV). High-resolution spectra were recorded at 45° take-off-angle by a concentric hemispherical analyzer operating in the constant pass energy mode at 29.35 eV, using a 720 μm diameter analysis area. Under these conditions the Au $4f_{7/2}$ line was recorded with 1.16 eV FWHM at a binding energy of 84.0 eV. The spectrometer energy scale was calibrated using Cu $2p_{3/2}$, Ag $3d_{5/2}$ and Au $4f_{7/2}$ photoelectron lines at 932.7, 368.3 and 84.0 eV, respectively. Charge referencing was done against adventitious carbon (C 1*s* 284.8 eV). The pressure in the analysis chamber was maintained $<5\times10^{-6}$ Pa. PHI ACCESS ESCA-V6.0 F software package was used for acquisition and data analysis. A Shirley-type background was subtracted from the signals. Recorded spectra were always fitted using Gauss–Lorentz curves in order to determine more accurately the binding energy of the different element core levels.

Surface acidity was investigated using a range of methods. IR spectra were recorded on a Protégé Magna Fourier Transformation Instrument, using both KBr and KBr-free pressed powder discs. Self-supported discs were activated in the IR cell by heating under vacuum at 813 K, pivalonitrile (t-C_4H_9CN) (1 Torr at equilibrium) was introduced at room temperature, then immediately evacuated at the same temperature to eliminate physisorbed species. Stepwise desorption was continued up to 573 K. A background spectrum was automatically subtracted each time. Diffuse reflectance UV–vis spectra were recorded with a Jasco V7 Instrument.

The total acidity was evaluated by temperature-programmed desorption of ammonia (NH_3-TPD). The samples were first heated in a He flow at 673 K to remove surface adsorbed species, before adsorbing ammonia at 373 K. NH_3-TPD was carried out between 373 and 773 K, at 10 K min^{-1}, with on-line gas chromatographic analysis (Shimadzu GC-14A).

The catalytic decomposition of *iso*propanol at 493 K was used as a test reaction for the study of the effective acidity. A fixed-bed tubular glass reactor working at atmospheric pressure was used for a solid charge of 30 mg without dilution. Samples were pretreated at 593 K in a helium flow for 3 h. *Iso*propanol was fed into the reactor by bubbling a flow of He (dried through a molecular sieve, flow rate 25 cm^3 min^{-1}) through a saturator-condenser at 303 K, which allowed a constant *iso*propanol flow of 7.5 vol%. None of the samples showed diffusion restrictions. The reaction products were analyzed by an on-line gas chromatograph (Shimadzu GC-14A) provided with a FID and a fused silica capillary column SPB1.

The catalytic isomerization of 1-butene was used as a further test for surface acidity. Tests were performed in a tubular glass flow microreactor. The samples were pretreated for 2 h in N_2 flow at 673 K, and experiments were performed at this temperature. The 1-butene was at 5% abundance in nitrogen. Any non-converted 1-butene, and the reaction products were analyzed on-line in a gas chromatograph (HP 5890 series II) equipped with a wide-bore $KCl/AlCl_3$ column. For this reaction, the distribution of *n*-butenes is near equilibrium and, consequently, the conversion is defined as the ratio [(products−*n*-butenes)/1-butene feed] × 100. The amount of coke was deduced from the weight loss of the recovered sample after burning in air in the range 363–1073 K, as measured by thermogravimetry.

3. Results and discussion

3.1. XRD and morphology

Powder X-ray diffraction patterns of materials recovered after removal of surfactant by thermal treatment at 823 K, are shown in Fig. 1. As observed for other heteroatom-doped silicas, the degree of long-range order as expressed by the number and breadth of low-angle diffraction peaks is highest in materials of moderate degree of substitution. In the present case, samples with Si/Zr of 40 or 30 clearly show 4 diffraction peaks before calcination, (corresponding, in a system of hexagonal symmetry, to diffraction from [100], [110], [200] and [210] planes). After calcination at 823 K, the [110] and [200] diffraction lines appear as a broad shoulder on the [100] peak. The data of Fig. 1 show that the degree of crystallinity of the as-synthesized materials is high. The materials prepared with the above-mentioned conditions show a similar crystallinity to that observed for the silica zirconia materials obtained by Lefebvre et al. [25] by using the same template but different zirconium and silicon sources. Regions of regular ordering of the pores into a hexagonal arrangement are directly observable in the transmission electron

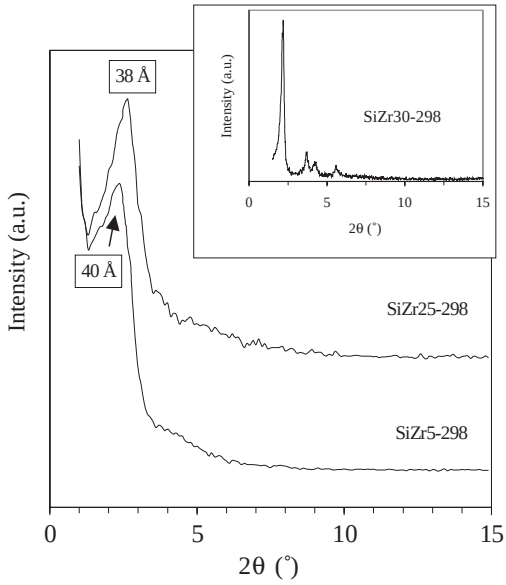

Fig. 1. XRD powder patterns of calcined Zr-doped mesoporous silica SiZr5-298 and SiZr25-298. Inset: non-calcined SiZr30-373.

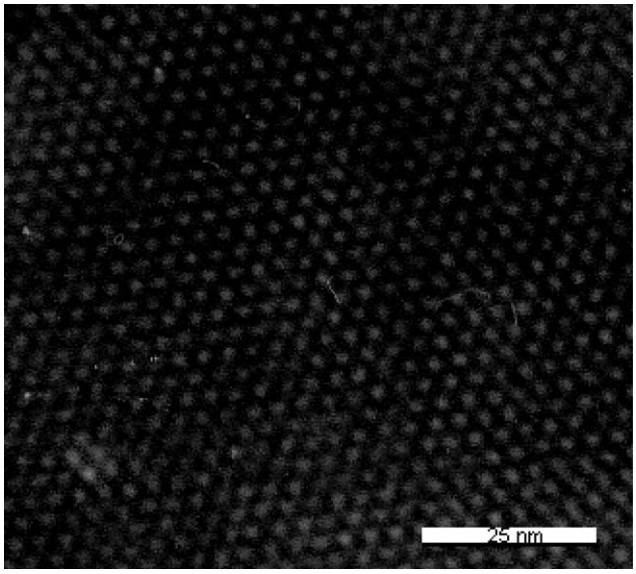

Fig. 2. Transmission electron micrograph of non-calcined SiZr30-373.

micrograph of Fig. 2. For materials with Si/Zr close to 5, a single diffraction peak was observed, with d_{100} values between 3.2 and 4.5 nm. Thus, the crystallinity decreases on increasing the amount of Zr incorporated in the silica framework, as previously observed by Ocelli et al. [31] for zirconium or titanium doped mesoporous silica. The unit cell dimension of materials prepared is sensitive to the temperature of reaction, since d_{100} increases, for example, from 4.03 nm (preparation at 298 K) up to 4.47 nm (423 K) for Si/Zr = 5. At identical reaction temperature, materials with low zirconium content have lower d_{100} than those with higher zirconium content; compare e.g., SiZr25-298 and SiZr5-298, or SiZr25-353 and SiZr5-353 and, in addition, the FWHM of the diffraction line is enlarged. The diffraction line given by Zr-MCM-41 materials is still visible, albeit less well-defined, after further heating at 1073 K. In no case was any diffraction evidence observed for the presence of crystalline segregated cubic or monoclinic ZrO_2, although this does not exclude the presence of a small particle, X-ray amorphous phase. The calcined zirconium-rich sample SiZr5-298 was also examined using atomic force microscopy, and typical images are shown in Fig. 3. At high magnification a "honeycomb" arrangement of the surface may be clearly observed, even in samples giving only a single diffraction line in XRD.

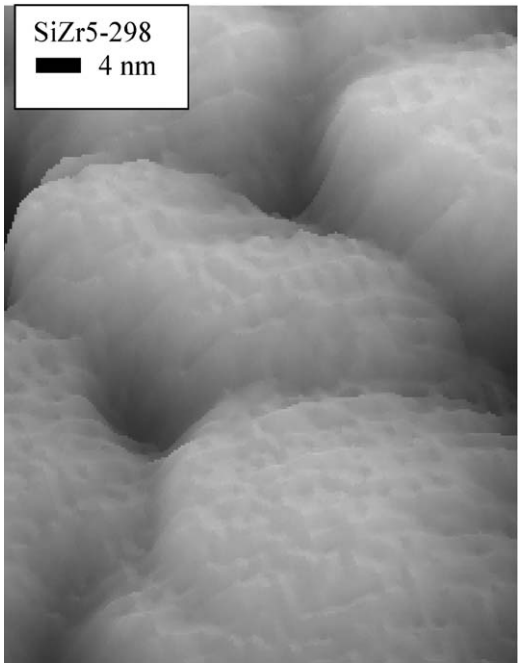

Fig. 3. Atomic force microscopic image of SiZr5-298.

Textural characteristics were evaluated from nitrogen adsorption–desorption isotherms at 77 K. As shown in Fig. 4, all the zirconium-containing materials exhibit reversible type IV isotherms in the IUPAC classification. They present a sharp inflection point at $P/P_0 = 0.35-0.40$, characteristic of capillary condensation within uniform mesopores. This uniformity is also shown by the narrow pore size distributions calculated by the Cranston and Inkley method for cylindrical pores. The coincidence of the adsorption and desorption branches can be ascribed to a similar mechanism for the two processes, which reflects the absence of adsorbate pore blocking. Indeed, the presence of any foreign species, such as extra-framework zirconium oxide, in the channels of the structure would be expected to lead to an irreversible isotherm with hysteresis. The BET specific

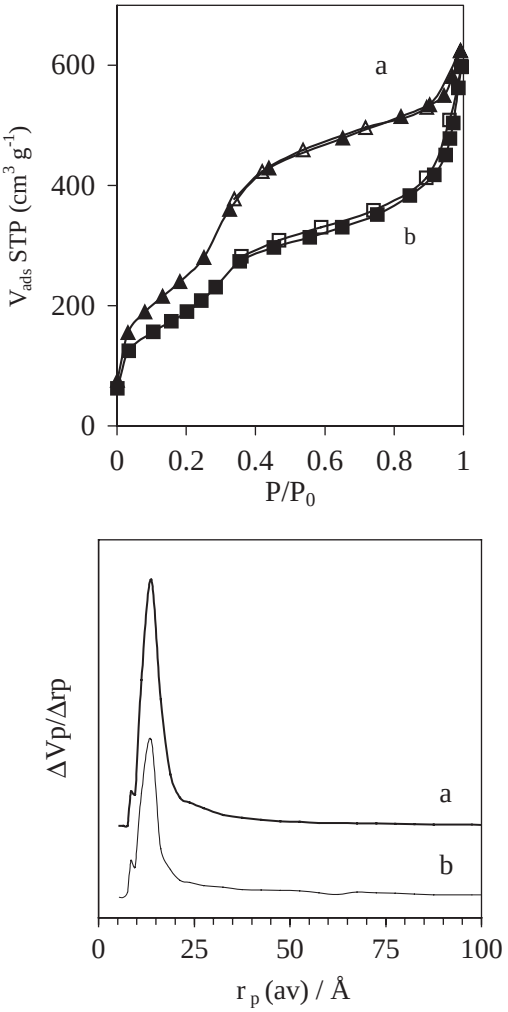

Fig. 4. N_2 adsorption-desorption isotherms at 77 K and the corresponding pore size distributions of (a) SiZr25-298 and (b) SiZr5-298.

surface areas and the accumulated pore volumes generally decrease as the zirconium content rises. Table 1 summarizes values of the textural parameters of the zirconium containing mesoporous silicas.

The average pore size of the non-doped silica compound after calcination at 1073 K is lower by 25% that of its value after calcination at 813 K. In contrast, zirconium-doped samples appear to be more resistant thermally, the average pore size being reduced only by 12–17%. Even after calcination at 1073 K, all materials retain their mesoporous character and a high surface area.

3.2. Skeletal FT-IR studies

The skeletal FT-IR spectra in the region 400–1500 cm^{-1} (Fig. 5) show the features typical of any silica-based material with a prominent shoulder at 1220 cm^{-1}, a main maximum at 1090 cm^{-1}, weak maxima at 968 and 800 cm^{-1}, and a strong band at 466 cm^{-1}. The two higher frequency components are due to the Si–O–Si asymmetric stretching vibrations, the band at 968 cm^{-1} to the Si–(OH) stretching of terminal silanols, the band at 800 cm^{-1} to the symmetric stretching/in plane deformation of Si–O–Si bridges and the maximum at 466 cm^{-1} to the rocking of the Si–O–Si bridges [36]. The addition of zirconium at first causes a shift to lower wavenumbers of all bands (the main maxima shift to 1080, 796 and 456 cm^{-1}) while the absorption in the region 930–1000 cm^{-1} increases in intensity although is now less well-resolved. This is probably due to the superimposition of stretching vibrations of Si–O and Si–O–Zr bonds, showing that Zr is incorporated, at least in part, into the silica network. Additionally a new broad absorption, which could be assigned to Zr–O stretching vibrations, is observed in the region 400–600 cm^{-1}, superimposed on the Si–O deformation bands. No features typical of zirconia polymorphs appear [36].

Table 1
Structural and textural characteristics of Zr-doped mesoporous silica

Sample	Si/Zr molar ratio	d_{100} (nm)	S_{BET} (m^2/g)	Vp (cm^3/g)	dp_{av} (nm)
SiZr25-298	25	3.84	854	0.63	3.9
SiZr25-353	25	3.17	1386	1.02	2.5
SiZr5-298	5	4.03	731	0.72	4.0
SiZr5-353	5	3.79	973	0.76	2.8
SiZr5-373	5	3.85	865	1.33	5.5
SiZr5-423	5	4.47	420		

3.3. X-ray photoelectron spectroscopic characterization

The results of XPS analyses are shown in Table 2 with those of bulk chemical analysis. In Fig. 6 the O 1*s*, Zr 2*p* and Si 2*p* core level spectra for sample SiZr5-298 are shown as an example. The bulk Si/Zr ratio determined by atomic absorption spectroscopy is in good agreement with that of the synthesis ratio. In contrast, XPS results show that the surface Si/Zr ratio is, in general, 1.5–4 times higher than that of the bulk. This is not unexpected, given the faster rate of hydrolysis of zirconium alkoxides compared with those of silicon and to the trend of zirconium ions to adopt a coordination number higher than four. In general, the O 1*s* peak becomes more asymmetric as the Zr content increases, indicating two different environments, Si–O–Si (at 533.0 eV) and Si–O–Zr (at 531.0 eV) (see Fig. 6). This further supports the incorporation of zirconium into the silica framework. The binding energy of O 1*s* is 0.7 eV higher than that giving by oxygen in ZrO_2 (530.2 eV), which indicates that if a segregated oxide phase of zirconium exists, it must be in only a negligible quantity.

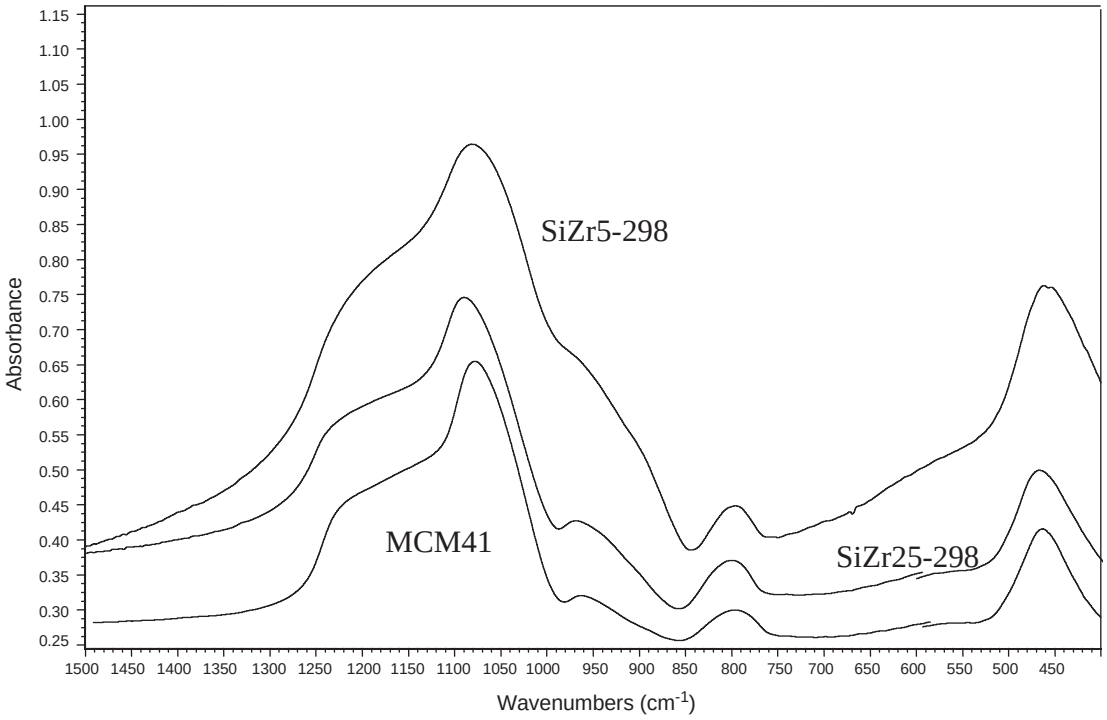

Fig. 5. FT-IR spectra of pressed discs of Zr-doped mesoporous silica powders (outgassed at 773 K).

Table 2
Binding energy (eV) and Si/Zr atomic ratio determined by XPS

Sample	Si/Zr synthesis ratio	Si/Zr AAS[a]	O 1s		Zr $3p_{3/2}$	Si 2*p*	Si/Zr XPS
SiZr25-298	25	23.2	531.0	1%	182.8	103.3	98.9
			533.0	99%			
SiZr5-298	5	4.8	531.0	14%	182.8	102.9	7.5
			533.0	86%			
SiZr5-373	5	4.9	531.0	11%	182.8	102.8	7.5
			532.8	89%			

[a] AAS = Atomic absorption spectroscopy.

3.4. Characterization by UV–vis spectroscopy

The UV–vis spectra, recorded in air without any pretreatment of the samples, are reported in Fig. 7. MCM-41 type silica materials do not absorb in either the UV or visible regions, but incorporation of Zr leads to absorption in the UV.

Pure zirconia polymorphs present different UV–vis spectra [35]. The absorption edge of zirconium oxide based powders is due to $O^{2-} \rightarrow Zr^{4+}$ charge transfer transitions, corresponding to the excitation of electrons from the valence band (having O 2*p* character) to the conduction band (having Zr 4*d* character). The coordination of zirconium in oxides varies generally from six-fold to eight-fold, with examples provided by perovskite-type $SrZrO_3$ (6-fold), baddeleyite-type zirconia (7-fold) and cubic zirconia and zircon, $ZrSiO_4$ (8-fold). The position of the edge shifts is located at lower energy for octahedral Zr^{4+} (inflection point near 300 nm for the perovskite), than for the heptacoordinated Zr^{4+} of monoclinic ZrO_2 (inflection point near 240 nm) [37]. For Zr^{4+} in coordination eight the edge is at the highest energy (inflection point near 220 nm). These data refer to bulk polymorphs, while different positions of the absorption bands are expected for isolated Zr polyhedra. On the other hand, according to Ciuparu et al. [38], defects in zirconia give rise to absorptions in the region 250–350 nm.

The Si–Zr sample SiZr25-298, with a low zirconium content, shows a broad and quite weak absorption with a maximum possibly split near 240 and 280 nm and a tail extending up to ca. 360 nm. The sample richest in zirconium, SiZr5-298, has a different spectrum, with a sharp feature near 210 nm, and broad bands of increasing strength at 275, 330 and 375 nm.

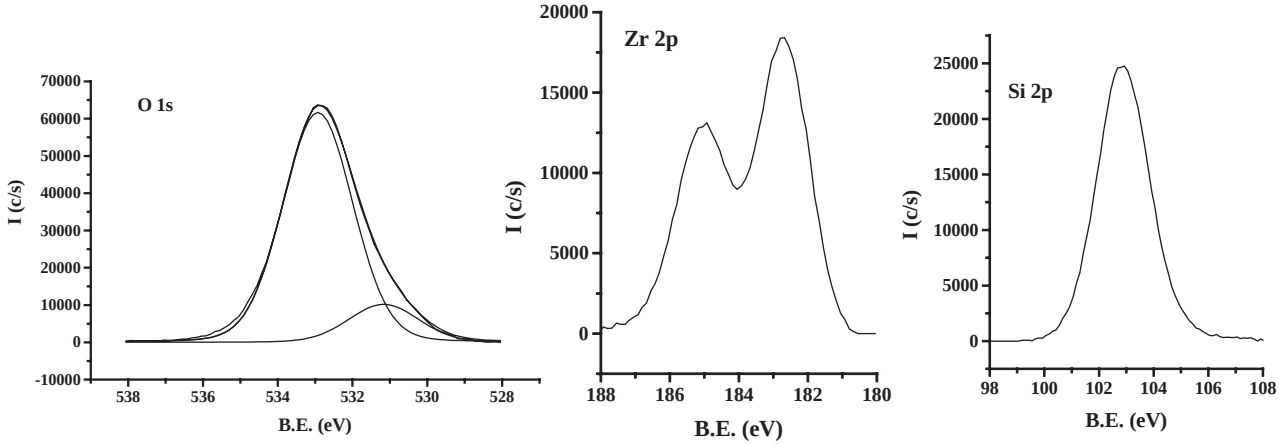

Fig. 6. O1*s*, Zr 3*d* and Si2*p* core level spectra for sample SiZr5-298.

These data show that bulk zirconia is not present in the sample SiZr25-298. The spectrum is compatible with that of nearly isolated Zr^{4+} cations with coordination 6 or 7. In sample SiZr5-298, the edge near 210 nm suggests the presence of small amounts of cubic or tetragonal ZrO_2-like particles. The absorptions in the range 250–350 nm should be assigned to $O^{2-} \rightarrow Zr^{4+}$ charge transfer transitions with Zr in low coordination states (possibly 6) either isolated or present in small Zr_xO_y clusters in the silica framework.

3.5. X-ray absorption spectroscopy

The local environment around zirconium was studied in a calcined material with Si/Zr ratio of 25 and prepared at 353 K, using X-ray absorption spectroscopy. The near-edge region of zirconium oxides is informative since the shape of the resonance above the absorption edge in compounds of local 6-, 7- or 8-fold coordination environment is rather characteristic [39–41]. Thus while a system of local octahedral surroundings gives a featureless, relatively narrow resonance, those of a local 7- or 8-fold environments are broader, with a shoulder to the low energy side of the principal resonance. In the present case, the shape at the absorption maximum of the spectrum in the near edge region of SiZr25-373 most closely resembles that of $ZrSiO_4$ (8-fold coordination), although it is also not very different from that given by monoclinic ZrO_2 (7-fold coordination) (Fig. 8). Confirmation of an 8-fold environment is provided by curve-fitting the contribution of the first shell of atoms to the total EXAFS spectrum. The results show the presence of about 5 oxygen atoms at 2.11 Å, and 3 oxygen atoms at 2.28 Å. These distances are close to those determined by EXAFS for the first coordination sphere of $ZrSiO_4$ (2.10 Å, 4 atoms; 2.22 Å, 4 atoms), and which agree with those reported from X-ray diffraction [42]. The second principal peak in the Fourier transformed EXAFS

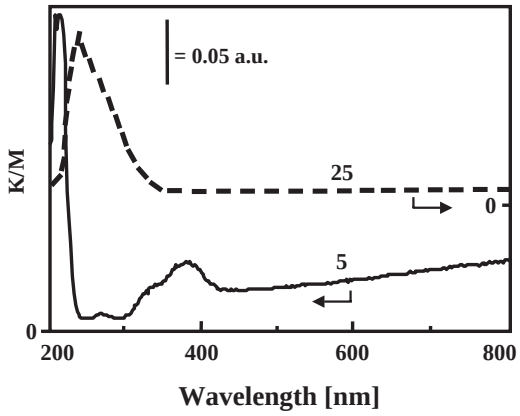

Fig. 7. UV–vis spectra of Zr-doped mesoporous silica powders. The Si/Zr ratio decreases downwards.

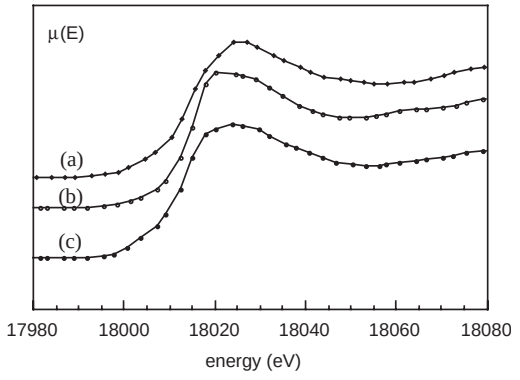

Fig. 8. Normalized X-ray absorption spectra in the near edge region of (a) ZrO_2, (b) $ZrSiO_4$ (c) ZrSi25-353.

spectrum was identified as arising from the couple Zr···Si, with 3 Si atoms located at 3.44 Å from zirconium, this distance being intermediate between those in $ZrSiO_4$ (2 Si at 2.99 Å, 4 Si at 3.68 Å, EXAFS results) (Fig. 8). However, the number of silicon neighbors is lower than expected. Simulation using

FEFF including multiple scattering contributions indicates the occurrence of constructive or destructive interference of EXAFS signals given by direct back-scattering from silicon, and those from a 2-leg path involving back-scattering via oxygen, depending on the value of the angle Zr–O–Si, and the interatomic distance. Destructive interference, which is highest for an angle Zr–O–Si around 140–145°, causes intensity reduction of the corresponding maximum in the Fourier transform (Fig. 9). For zirconium-doped mesoporous silica, angles around zirconium are expected to be different from this value, by comparison with the situation in $ZrSiO_4$. Thus, while this phenomenon might account partially for the low number of nearest neighbors, probably the most probable explanation lies in the location of the zirconium atom preferentially at the surface of the pores. In the case of isomorphous substitution of silicon by zirconium within the pore wall, the second nearest neighbor environment would be composed of 4 backscatters instead of 3. Thus EXAFS results provide strong evidence for supposing that in mesoporous silica-zirconia with Si/Zr of 25, the zirconium is mostly at the surface, such that a strong proportion of the oxygen atoms bonded to zirconium correspond to surface non-condensed oxygen atoms. This result is not unexpected since zirconium exhibits a strong tendency to high coordination numbers [6–8] especially against small ligands such as F^-, O^{2-}. When Zr is hosted in a SiO_2 structure, this tendency to high coordination is maintained, and so, zirconium atoms may migrate to the surface during the synthesis process. This situation, associated with the high coordination of zirconium, is responsible for the acidic properties of the system, described below.

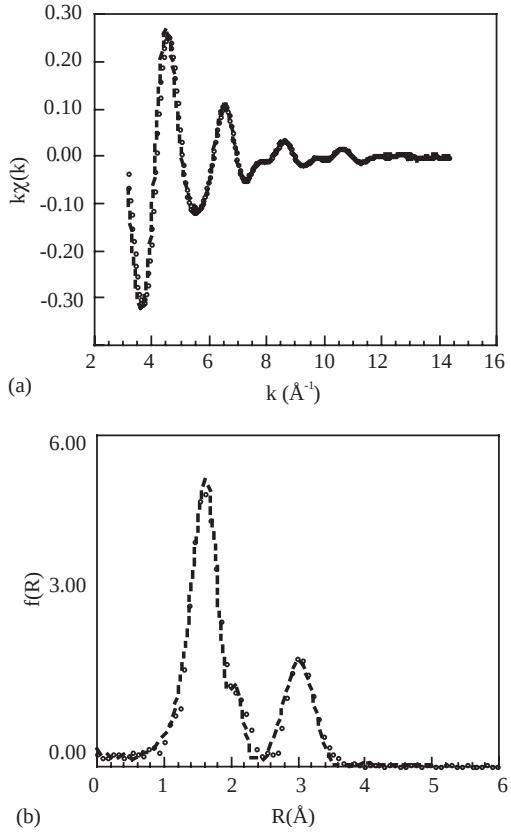

Fig. 9. Experimental (○ ○ ○ ○) and calculated (-------) EXAFS spectra in (a) *k*-space, (b) *R*-space. Spectra were calculated with Zr–O: $N = 4.8$; $R = 2.11$ Å, $\sigma = 0.07$ Å; Zr···O: $N = 3.2$, $R = 2.28$ Å, $\sigma = 0.07$ Å, Zr···Si: $N = 3.1$, $R = 3.44$ Å, $\sigma = 0.07$ Å.

3.6. Surface acidity characterization by IR spectroscopy

The surface acidity of the MCM-41 type silica-zirconia samples has been investigated using pivalonitrile as a probe, as well as by study of the IR spectra of the surface hydroxy groups. The CN- stretching mode of pivalonitrile shifts upward by interaction with the electron-withdrawing Lewis and Brønsted acid sites. Moreover, the extent of the shift of the OH stretching band caused by H-bonding of the nitrile with surface OHs can be taken as a measure of the strength of such OH groups as Brønsted acid sites [43,44]. In all cases (Fig. 10) a single and sharp OH stretching band centered at $3742 \pm 2\,cm^{-1}$, due to terminal silanol groups is observed. After outgassing at 673–773 K no other individual bands are seen. The breadth of the main component and the typical tail it shows towards lower

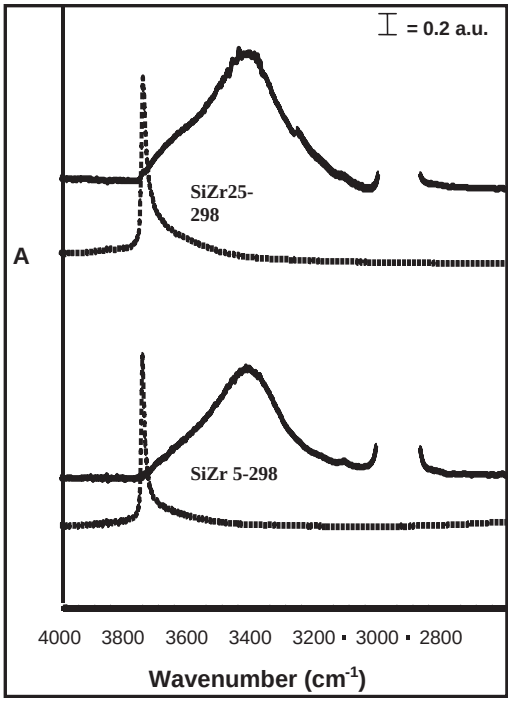

Fig. 10. FT-IR spectra in the OH stretching region of pressed discs of Zr-doped mesoporous silica after contact with vapor (full lines) and after subsequent outgassing (broken line).

frequency strongly decreases on increasing the Zr content.

On contact with pivalonitrile, an almost complete perturbation of the sharp silanol band occurs, with a strong downward shift and broadening, due to the formation of hydrogen bonds (Fig. 10). The perturbed position is near $3410 \pm 10\,cm^{-1}$ irrespective of the Zr content, with possibly a weaker broad component near $3600\,cm^{-1}$. The perturbed position seems to be the same for the samples SiZr25-298, and SiZr5-298, and is just the same as observed for pure mesoporous silica [45]. This indicates that the Brønsted acidity of the silanol groups is substantially unmodified by zirconia addition, but it is not excluded that the acid strength of some of the silanols groups is a little increased due to the neighboring zirconium sites.

The spectra in the C≡N stretching region (Fig. 11), recorded in the same conditions, allow identification, in all cases, of the presence of medium-strength Lewis acid sites, responsible for the observed coordinative adsorption of pivalonitrile, characterized by the CN stretching band at $2276 \pm 2\,cm^{-1}$. In contrast, the bands at 2235 and $2248\,cm^{-1}$ are due to pivalonitrile molecules only slightly perturbed by hydrogen bond formation. The Brønsted to Lewis acid site ratio changes strongly on increasing Zr content, as shown by the CN stretching intensity ratio $I_{2235+2248}/I_{2275}$. On the other hand, the

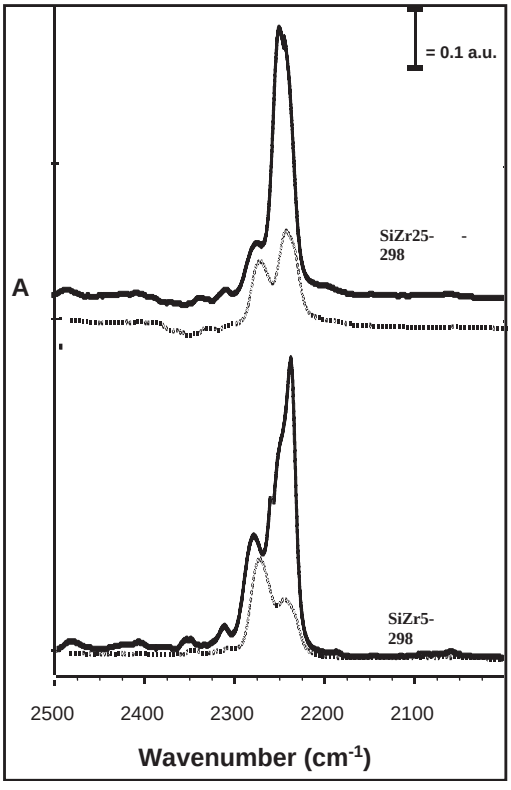

Fig. 11. FT-IR spectra in the CN stretching region of pressed discs of Zr-doped mesoporous silica after contact with vapor (full lines) and after subsequent outgassing (broken line).

I_{2248}/I_{2235} intensity ratio also changes in the same way, possibly indicating that two families of silanol groups actually exist, one of them being more acidic, and that the abundance of these more acidic groups increases on increasing Zr content. These data also indicate that these materials are very weak as Brønsted acids but carry a significant medium-strong Lewis acidity provided by coordinatively unsaturated Zr^{4+} cations.

3.7. Total surface acidity by temperature-programmed desorption of ammonia (NH_3-TPD)

Ammonia TPD is widely used to determine the total acidity of solids. The amount of ammonia desorbed at some characteristic temperatures is taken as a measure of the number of acid centers while the temperature range in which the ammonia is desorbed is an indicator of the strength of the acid sites. For mesoporous silica-zirconia, the NH_3-TPD curves are broad and complete desorption is not reached even at 673 K (Fig. 12). The amount of ammonia desorbed between 373 and 673 K is lower than that calculated by assuming that each zirconium atom is associated with an acid site. This difference may be due to the presence of strong acid sites, or to the location of a part of the zirconium atoms within the pore walls, and hence being inaccessible to NH_3 molecules. For example, the sample SiZr5-298 has an experimental value of $1160\,\mu mol\ NH_3\,g^{-1}$, is lower than the calculated value of $2237\,\mu mol\ NH_3\,g^{-1}$ by almost a factor 2. The total acidity determined for these compounds is comparable to those of pillared clays and zeolites [46,47]. In similar experiments, the acidity of Al-MCM-41 silica was measured as $758\,\mu mol\ NH_3\,g^{-1}$ and in the case of pure MCM-41 was only $680\,\mu mol\ NH_3\,g^{-1}$.

3.8. Characterization of the surface acidity by catalytic reactivity

3.8.1. Isopropanol dehydration

This reaction can be regarded as one typical for the investigation of the effective catalytic properties of acid centers in metal oxides, and catalysts can be classified

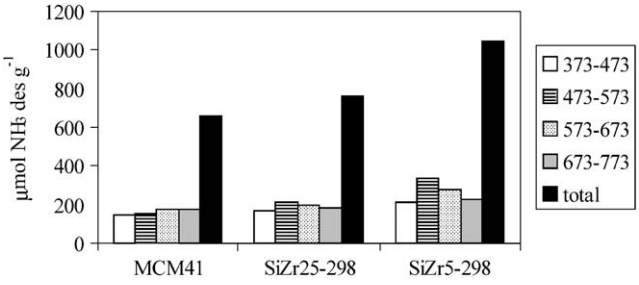

Fig. 12. NH_3-TPD of Zr-doped mesoporous silica.

Table 3
Activity in 1-butene isomerization for silica, Al and Zr-doped MCM41-type solids

Sample	Compos.	S_{BET} (m^2/g)	Conv. (%)	coke	*i*-butene (%)	*i*-butane (%)	*n*-butane (%)	C5+ (%)
MCM-41	SiO_2	1281	4.7	0	2.8	0	0	0
AlMCM-41	Si/Al = 5	925	5.4	1.5	3.0	0	0	0.1
SiZr5–298	Si/Zr = 5	731	17.7	0.1	13.8	0.2	0.1	1.3

with regard to their propensity toward dehydration or the dehydrogenation activity to propene or to acetone, respectively. Whilst siliceous MCM-41 is not active in this reaction, zirconium-doped samples displayed a high catalytic activity ($30\,\mu mol\,g^{-1}\,s^{-1}$ at 473 K for sample SiZr5-298) and a selectivity of 99% to propene, which was maintained after 20 h of reaction. This reactivity toward the dehydration reaction is expected to be associated with the Lewis acidity of these materials [48].

3.8.2. 1-butene isomerization

To further investigate the acidity of these materials, the catalytic isomerization of 1-butene was chosen as test reaction [49,50]. The formation of isobutene (skeletal isomerization) needs stronger Brønsted acid sites ($H_R < -663$) than those required for isomerization or double bond migration ($0.82 > H_R > -4.04$). The reaction occurs on Brønsted acid sites via carbenium ion intermediates by a three-step mechanism. Isomerization of 1-butene is considered to be catalyzed mainly by Brønsted acid sites. As shown in Table 3, the zirconium-containing sample is much more active than either MCM-41 or Al-MCM-41, suggesting an increase number of Brønsted sites in the former. In fact the Si/Zr sample produces a higher amount of the skeletal isomerization reaction product, isobutene, with a good conversion. This is in agreement with the small strengthening effect on Brønsted acidity identified from IR experiments. The zirconium-containing sample also shows higher activity than the aluminum-doped sample considered as a reference. On the other hand, the Al-containing sample produces much more coke than the zirconium-containing samples. Coking is probably responsible for significant deactivation of the catalyst during time on stream. No coke was detected on the Zr-containing samples, showing that it has much less strong Brønsted acid sites than the Al-containing sample, in agreement with IR studies.

4. Conclusions

One of the considerations of key importance in the context of substitution of silicon by a heteroatom in doped MCM-41 type silica is the extent to which the heteroatom is effectively incorporated into the structure, or whether partial phase segregation occurs. Conclusions from the analysis of EXAFS and XPS data, as well as UV–vis spectra, of mesoporous silica zirconia are convergent, and indicate that zirconium is dissolved into the silica matrix to give a single phase material, but with enrichment at the pore surfaces. Thus the EXAFS results indicate that zirconium atoms have a coordination number of 7 or 8, compatible with preferential location of zirconium at the pore surfaces. Under such conditions, a high proportion of the surrounding oxygen corresponds to surface non-condensed oxygen atoms resulting in augmentation of the surface acidity. Thus the total acidity is much enhanced with respect to pure siliceous MCM-41, reaching a value of $1160\,\mu mol\ NH_3\,g^{-1}$ for SiZr5-298. IR studies of adsorbed pivalonitrile identify the surface acid sites as medium strong Lewis acid centers, and only weakly Brønsted acidic. The surface area decreases as the zirconium content increases, such that the density of surface acid sites (number of surface acid sites/unit area) increases significantly. Such characterization of the nature, strength and number density of acid sites is of relevance to the application of these materials as catalysts, and the results of further investigations on these aspects will be reported subsequently.

Acknowledgments

This work has been supported by the European Union (GROWTH programme, contract GR5D-2001-00537), CICYT (Spain project MAT 2000-1144) and Acciones Integradas Spain-France (Picasso programme, project no. HF2000-0139).

References

[1] R.M. Barrer, Zeolites and Clay Minerals as Sorbents and Molecular Sieves, Academic Press, London, 1978.
[2] P. Meriaudeau, C. Naccache, Adv. Catal. 44 (2000) 505.
[3] R. Szostac, Molecular Sieves, Blackie Acad, London, 1998.
[4] N.Y. Chen, W.E. Garwood, F.G. Dwyer, Shape Selective Catalysis in Industrial Applications, 2nd Edition, Dekker, New York, 1996.
[5] P.B. Venuto, Micropor. Mesopor. Mater. 2 (1994) 297.
[6] C.T. Kresge, M.E. Leonowicz, W.J. Roth, J.C. Vartuli, J.S. Beck, Nature 359 (1992) 710.
[7] J.S. Beck, J.C. Vartuli, W.J. Roth, M.E. Leonowicz, C.T. Kresge, K.D. Schmitt, C.T.W. Chu, D.H. Olson, E.W. Sheppard, S.B.

McCullen, J.B. Higgins, J.L. Schlenker, J. Am. Chem. Soc. 144 (1992) 10834.
[8] M.J. Meziani, J. Zajac, D.J. Jones, S. Partyka, J. Rozière, Langmuir 16 (2000) 2262.
[9] A. Corma, Chem. Rev. 97 (1997) 2373.
[10] A. Sayari, Chem. Mater. 8 (1996) 1840.
[11] P.B. Venuto, Stud. Surf. Sci. Catal. 105 (1996) 811.
[12] J. Medina-Valtierra, M.A. Sanchez, J.A. Montoya, J. Navarrete, J.A. de los Reyes, Appl. Catal. A: General 158 (1997) L1–L6.
[13] S. Morin, P. Ayrault, S. El Mouahid, N.S. Gnep, M. Guisnet, Appl. Catal. A: General 159 (1997) 317.
[14] R. Raja, J.M. Thomas, G.J. Sankar, Chem. Commun. (1997) 525.
[15] J.M. Thomas, R. Raja, G. Sankar, R.G. Bell, Nature 398 (1999) 227.
[16] D. Hamon, M. Vrinat, M. Breysse, B. Durand, F. Beauchesne, T. des Courières, Bull. Soc. Chim. Belg. 108 (1991) 933.
[17] V. Indovina, M. Occhiuzzi, P. Ciambelli, D. Sannino, G. Ghiotti, F. Prinetto, Stud. Surf. Sci. Catal., in: J.W. Hightower, W.N. Delgass, E. Iglesia, A.T. Bell (Eds.), 11th Intenational Congress on Catal., Vol. 101, Elsevier, Amsterdam, 1996, p. 691.
[18] K. Arata, Adv. Catal. 37 (1990) 165.
[19] D.G. Barton, S.L. Soled, G.D. Meitzer, G.A. Fuentes, E. Iglesia, J. Catal. 181 (1999) 57.
[20] D.J. Jones, J. Jiménez-Jiménez, A. Jiménez-López, P. Maireles-Torres, P. Olivera-Pastor, E. Rodríguez-Castellón, J. Rozière, Chem. Commun. (1997) 431.
[21] A.O. Bianchi, M. Campanati, P. Maireles-Torres, E. Rodríguez-Castellón, A. Jiménez-López, A. Vaccari, Appl. Catal. A: General 220 (2001) 105.
[22] A. Jiménez-López, E. Rodríguez-Castellón, P. Maireles-Torres, L. Díaz, J. Mérida-Robles, Appl. Catal. A: General 218 (2001) 295.
[23] P. Braos-García, L. Díaz, E. Rodríguez-Castellón, P. Maireles-Torres, A. Jiménez-López, Studies Surf. Sci. Catal. 135 (2001) 237.
[24] R. Moreno-Tost, J. Santamaría-González, P. Maireles-Torres, E. Rodríguez-Castellón, A. Jiménez-López, Appl. Catal. B. 38 (2002) 51.
[25] X.X. Wang, F. Lefebvre, J. Patarin, J.M. Basset, Micropor. Mesopor. Mater. 42 (2001) 269.
[26] Z. Luan, L. Kevan, J. Phys. Chem. B 101 (1997) 2020.
[27] S. Biz, M.L. Occelli, Catal. Rev. Sci. Engng. 40 (1998) 327.
[28] A. Tuel, S. Gontier, R. Teissier, Chem. Commun. (1996) 651.
[29] K. Chaudari, R. Bal, D. Srinivas, A.J. Chandwadkar, S. Sivasanker, Micropor. Mesopor. Mater. 50 (2001) 209.
[30] M.S. Hong, W.C. Huang, J.Y. Ying, Chem. Mater. 14 (2002) 1961.
[31] M.L. Ocelli, S. Biz, A. Aroux, Appl. Catal. A: General 183 (1999) 231.
[32] R.W. Cranston, F.A. Inkley, Adv. Catal. 9 (1957) 143.
[33] A. Michalowicz, in: Logiciels pour la Chimie, Société Française de Chimie, Paris, 1991, p. 102.
[34] B. Ammundsen, D.J. Jones, J. Rozière, F. Villain, J. Phys. Chem. 102 (1998) 7939.
[35] S.I. Zabinsky, J.J. Rehr, A. Ankudinov, R.C. Albers, M.J. Eller, Phys. Rev. B 52 (1995) 2995.
[36] E. Astorino, J. Peri, R.J. Willey, G. Busca, J. Catal. 157 (1995) 482.
[37] E. Fernández Lopez, V. Sanchez Escribano, M. Panizza, M.M. Carnasciali, G. Busca, J. Mater. Chem. 11 (2001) 1891.
[38] D. Ciuparu, A. Ensuque, G. Shafeev, F. Bozon-Verduraz, J. Mater. Sc. Lett. 19 (2000) 931.
[39] D.J. Jones, J. Rozière, in: M.C. Fairbanks, A.N. North, R.J. Newport (Eds.), Neutron and X-ray Scattering: Complementary Techniques, Institute of Physics Conference Series, Vol. 101, Bristol, UK, 1990, pp. 405–407.
[40] D.J. Jones, J. Rozière, in: S.M. Hasnain (Ed.), X-ray Absorption Fine Structure Ellis Horwood, Chichester, UK, 1991, pp. 405–407.
[41] C. Sanchez, M. In, J. Non-Cryst. Solids 1 (1992) 147.
[42] K. Robinson, G.V. Gibbs, P.H. Ribbe, Am. Min. 56 (1971) 782.
[43] G. Busca, Catal. Today 41 (1998) 191.
[44] P.O. Scokart, P.G. Rouxhet, J. Colloids Interface Sci. 80 (1982) 96.
[45] M. Trombetta, G. Busca, M. Lenarda, L. Storaro, M. Pavan, Appl. Catal. A: General 182 (1999) 225.
[46] X. Tang, W.Q. Xu, Y.F. Shen, S.L. Suib, Chem. Mater. 7 (1995) 102.
[47] D. Zhao, Y. Yang, X. Guo, Zeolites 15 (1995) 58.
[48] M. Trombetta, G. Busca, M. Lenarda, L. Storaro, R. Ganzerla, L. Piovesan, A. Jimenez-Lopez, M. Alcantara-Rodríguez, E. Rodríguez-Castellón, Appl. Catal. A: General 193 (2000) 55.
[49] A. La Ginestra, P. Patrono, M.L. Berardelli, P. Galli, C. Ferragina, M.A. Massudi, J. Catal. 103 (1987) 346.
[50] P. Patrono, A. La Ginestra, G. Ramis, G. Busca, Appl. Catal. A 107 (1994) 249.